GEOPHYSICAL RESEARCH LETTERS, VOL. 27, NO. 5, PAGES 609-612, MARCH 1, 2000

Winter Clouds over the North Martian Polar Cap

Gordon H. Pettengill* and Peter G. Ford
Center for Space Research, Mass. Inst. of Technology

Abstract. The Mars Orbiter Laser Altimeter (MOLA) experiment, carried on the Mars Global Surveyor spacecraft, has observed echoes from cloud tops on roughly 2.5% of the total data taken above 70° N over the northern winter Martian polar hood from March to June 1998. Sloping wavefronts are commonly seen at latitudes above 70° N, implying the presence of propagating buoyancy waves. Since these wavefronts frequently extend from the surface up to 10 km at a time when CO_2 is known to be condensing on the polar surface, it seems likely that the laser-scattering particles consist primarily of CO_2 ice, and that the near-surface temperature lapse rate is 0.85 K / km, set by the vapor pressure of dry ice. From the observed wavelengths, where available, we have calculated the corresponding phase velocities; some of these waves appear to be correlated with surface discontinuities, and may represent lee waves.

1. Introduction

As part of its year-long sequence to reach a low-altitude, near-polar, circular mapping orbit by aerobraking, the Mars Global Surveyor [*Albee et al.*, 1998] spent 6 months from March to September 1998 in an elliptical holding orbit around Mars, called the Science Phasing Orbit (SPO). During the first four months of this time, while the spacecraft waited for the desired orientation of its orbital plane with respect to the sun, the Mars Orbiting Laser Altimeter (MOLA) instrument [*Zuber et al.*, 1992; 1998] was operated for a 25-minute interval surrounding periapsis on each $11^h\ 37^m$ orbit of the planet. It was fortunate that during this period the 170-km-high periapsis migrated slowly across the northern pole during the late winter and early spring, allowing an excellent opportunity to observe laser echoes from the tops of the dense polar-hood clouds characteristic of that season and latitude. About 2.5% of the total data obtained in this region were from clouds.

Clouds have long been known to exist on Mars, and were studied extensively during the Viking missions to that planet in the late 1970's [e.g. *Kahn*, 1984]. Of particular importance was the observation by barometers on the Viking landers of the seasonal deposition of a significant portion of the planetary CO_2 atmosphere on to the polar caps [*Hess et al.*, 1980]. Because sunlight is lacking during much of the polar winter, it was not feasible for the Viking orbiter to visually observe either the winter surface or the overlying clouds. The MOLA instrument, however, which carries its own illumination, has now shed light on the nature of these features.

2. Observations

As it flew over the north polar region at about 4.5 km s^{-1}, MOLA transmitted an 8-ns burst of 1.06μ m-wavelength infrared radiation towards the nadir every 0.1s, illuminating surface spots that varied in size from approximately 50m up to over 150m in dia., depending on the spacecraft altitude. Individual measurements were spaced about 450m apart along track.

The first returning echo that exceeded a preset threshold latched a round-trip timer and yielded a corresponding distance measurement. Thus, it was impossible to detect an echo from both a cloud top and the planetary surface beneath (or even a second echo deeper in the cloud) from the same transmitted pulse. Since the pulse is short (equivalent to 1.2m in range), echoes from a sharply defined planetary surface are far more efficiently detected than those from the "fuzzy" interface characteristic of most cloud tops; fortunately, the latter return earlier and so may pre-emptively trip the detector, if strong enough. The echoes themselves, of course, cannot distinguish the composition of the echoing material.

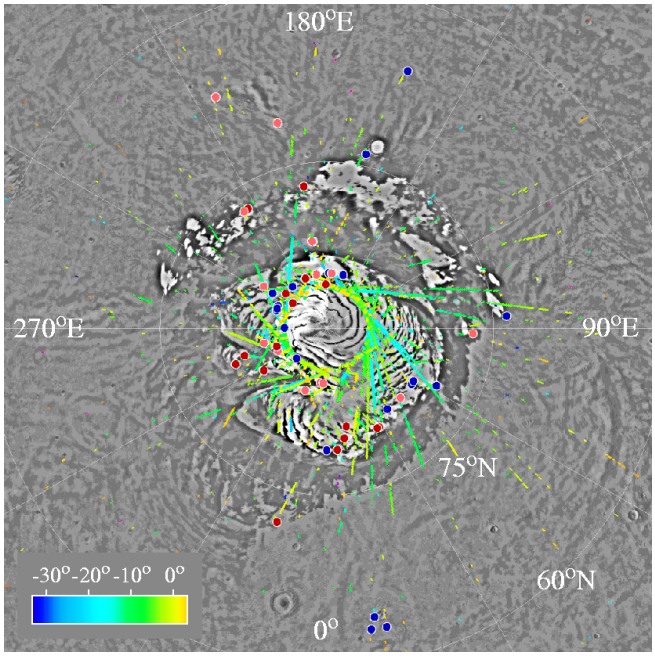

Figure 1. Plan view of the location of all cloud echoes seen during the SPO period. Colors in the bar indicate the solar horizon angle at the time of observation (positive values correspond to the sun above the local horizon). White encircled colored dots show the location of isolated clouds (Table 3). The dot color assignment is blue for those wavefronts with phase velocities in the same directional sense as the polar vortex winds (in the same direction as the surface rotational motion); red for those moving against the winds; and pink for those with an amorphous structure that cannot be analyzed in terms of a buoyancy wave.

* Also at the Department of Earth, Atmospheric, and Planetary Sciences, MIT.

Page number 1999GL010896
0094-8276 / 00 / 1999GL010896$05.00

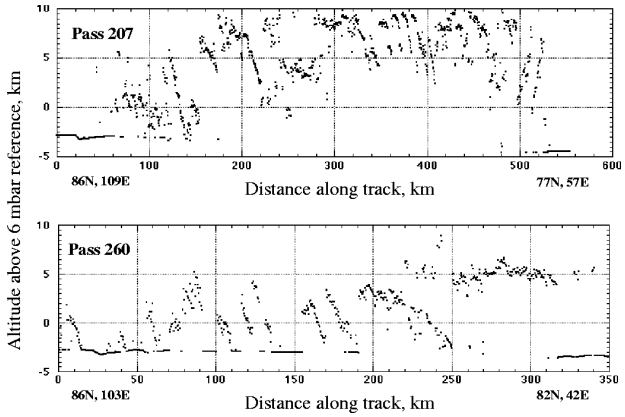

Figure 2. Examples of periodic cloud echo profiles from orbital passes 207 (L_S=301.3°) and 260 (L_S=316.4°). The discontinuous solid line seen below the clouds corresponds to echoes from the surface, which are often preempted by echoes from the clouds above.

Figure 1 shows the location of all major cloud echoes seen during the SPO, with detailed profiles from orbital passes 207 and 260 given in Figure 2. Of special interest are the many sloping cloud tops that extend from the surface to altitudes of 5 km and above. It is possible that even the clouds in pass 207, which show no echoes below about 4 km altitude in the central portion of the cloud mass, also extend to the surface, and that the lower regions, along with the surface, are obscured by echoes from overlying clouds.

It seems likely that the linear cloud-echo strings represent the sloping wavefronts of propagating buoyancy or gravity waves [*Holton*, 1992]. The existence of coherent wavefronts, extending up from the surface to altitudes of at least 10 km during the depths of winter (L_s = 301.3° and 316.4° for passes 207 and 260, respectively), when atmospheric CO_2 is known to condense at the pole [*Hess et al.*, 1980], suggests that the reflecting material consists of particles of dry ice which are alternately condensed and evaporated as the ambient temperature is modulated below and above the local freezing point by the passing buoyancy wave. These particles mark the condensation phase of the wavefront. If this is the case, then the vertical temperature profile, at least up to 10 km altitude, must follow that of a ``wet'' adiabat (see Appendix) for CO_2 ice, as shown in Figure 3. Relevant characteristics of the Martian winter surface and atmosphere are given in Table 1.

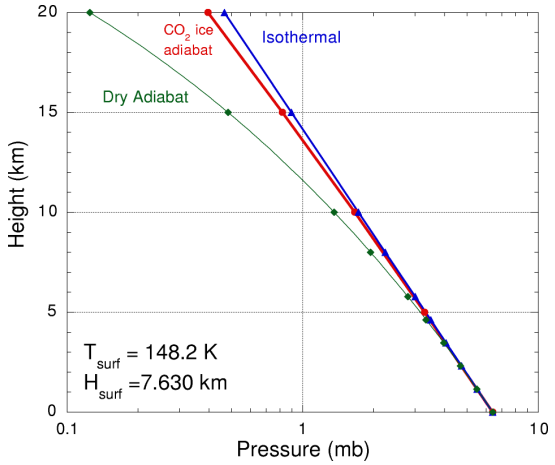

Figure 3. Possible profiles of atmospheric pressure above the winter Martian poles. The curves have been calculated 1) for a dry CO_2 adiabat with a lapse rate of 4.3° K km^{-1}; 2) a "wet" CO_2 adiabat following the vapor pressure of dry ice with a lapse rate of 0.85° K km^{-1}; 3) an isothermal temperature profile (zero lapse rate). The surface value of scale height assumed was 7.63K km^{-1}, at a temperature of 148.2K.

Table 1: Winter polar near-surface characteristics

Pressure, P_0, at reference geoid	6.0 *mbar*
Temperature, T_0, at ref. geoid	148.2 *K*
Accel. of gravity, *g*, at ref. geoid	3.72 ms^{-2}
Scale height, $H_o = kT_o/Mg$	7.63 *km*
"Wet" adiabatic lapse rate	0.85 $K\ km^{-1}$
Dry adiabatic lapse rate, $L_d = g/c_p$	4.3 $K\ km^{-1}$
Buoyancy frequency, $N = \sqrt{(L_d - L_w)\, g/T_0}$	9.31 10^{-3} $rad\ s^{-1}$

3. Particle Densities and Energetics

From the observed cloud echo strengths, assuming a geometric albedo of unity, we calculate that the reflecting regions comprise particle number densities of about $2 \times 10^8\, r^{-2} m^{-3}$, where *r* is the particle radius in μ m.The scattering particle radius is not well determined, but must be larger than 0.1 μ m in order to scatter the incident infrared radiation efficiently (below this size, the scattering cross section enters the Rayleigh limit of the Mie scattering law [*Mie*, 1908], and begins to drop off as the fourth power of the radius). On the upper end, the size is limited by the ability of the atmosphere to suspend the particles. Murphy *et al.* [1990] show that dust particles of density 2500 kg m^{-3} (roughly comparable to dry ice, which has a density of 1560 kg m^{-3}) cannot exceed about 50 μ m, if they are not to fall faster than 0.5 m s^{-1} in the Martian atmosphere and destroy the sharply defined wavefront during the intrinsic oscillation period of a typical gravity wave in the Martian environment of between half and one hour. [Tables 2 and 3]We assume a nominal radius of 1.0 μ m, which

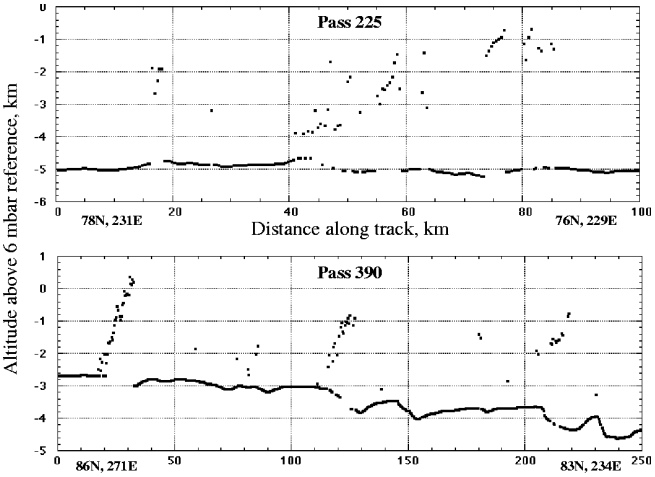

Figure 4. Echo profiles for isolated clouds observed over surface discontinuities on orbital passes 225 (L_S=306.5°) and 390 (L_S=350.7°).

Table 2: Characteristics of MOLA-observed clouds—that may correspond to periodic buoyancy waves. The intrinsic oscillation period is given by $2\pi/\hat{\nu}$ (see Appendix). The "extent" column estimates the overall length of the total periodic wave packet.

MGS Orbit Number	Lat ° N	Lon ° E	Intrinsic Oscillation Period (s)	Horizontal Structure			Vertical Structure			
				Extent km	λ_x km	c_x m s^{-1}	Min km	Max km	λ_z km	c_z m s^{-1}
207	81	65	1357	72	9.2	3.4	6.4	13.2	4.0	1.9
221	82	203	2139	45	17.9	4.2	7.0	14.1	5.4	1.4
222	84	44	1351	119	9.1	3.4	0.9	12.4	4.0	1.9
222	81	29	2885	83	9.8	1.7	4.4	9.6	2.2	0.4
224	85	73	1798	93	30.0	8.3	3.3	7.6	10.5	3.4
226	86	115	1174	122	11.6	4.9	2.8	14.7	5.5	3.5
233	82	318	1298	30	5.4	2.1	3.0	11.2	2.4	1.2
257	85	214	3414	140	64.8	9.4	1.3	5.9	12.6	1.9
260	85	62	1730	83	19.7	5.6	1.1	8.1	7.1	2.4
261	84	241	2144	109	10.4	2.4	1.3	7.8	3.1	0.8
330	82	2	1819	107	38.3	10.4	5.2	11.5	13.2	4.2
332	81	19	4535	64	40.1	4.4	4.7	9.1	5.9	0.7
351	82	28	5834	254	25.8	2.2	6.6	10.4	3.0	0.3

leads to a particle density of about 2×10^8 m^{-3} for the cloud tops, and assume that the condensation is controlled by the limited number of available nuclei. These assumptions allow the slightly supercooled gas to follow a dry adiabatic excursion (Figure 3) around the mean profile of a wet adiabat as the perturbed parcel oscillates up and down. Note that there would be no restoring force, and thus no wave, if the parcel tracked the ambient wet adiabat. The corresponding heat of fusion (6×10^5 j kg^{-1} at T=148K) associated with forming the estimated number densities is approximately 0.2% of that required to raise the temperature of the ambient gas by 0.1K, so the effect on the equation of state of the surrounding gas is negligible, provided the energy in a typical buoyancy wave is equivalent to 0.1K or more. Since the volume of the precipitate relative to its cross-section increases directly as its radius, even 50 μm particles could be accommodated. It seems likely, therefore, that a trivial fraction of the energy in the propagating wave is invested in the precipitation of the "marker" particles that are observed by MOLA.In the profiles of Figure 2, there do not appear to be any sharp discontinuities in surface relief associated with the wave structures, although it is possible that some have been missed because of obscuration by the overlying clouds. Cases of isolated clouds over surface discontinuities are common, however; Figure~4 shows several examples drawn from passes 225 and 390. It is probable that some of these isolated structures represent stationary lee waves, excited by winds deflected upward as they strike surface relief. The kinetic energy content of a typical polar surface wind blowing at ~10 m s^{-1}. [*Zurek et al.*, 1992] is 50 j kg^{-1}, enough to raise the ambient temperature by 0.06K if fully converted to thermal energy. But as shown above, only a small fraction of this (~0.3%) may be needed to produce the observed condensation. Since only a single wavefront is seen in most cases, it is not possible to determine the horizontal wavelength and thus the corresponding horizontal phase velocity. But, the observed tilt of the wavefront permits a calculation of the intrinsic oscillation (see Appendix). The distribution of isolated clouds is shown in Figure 1.

Since the MOLA data yield profiles only along the direction of spacecraft motion, we cannot determine the true wavelength in the absence of information on the wave propagation direction. Thus, the measured horizontal wavelength represents only an upper limit to the true value; the vertical wavelength, however, is unaffected. Since the vertical wavelength is always smaller (typically much smaller) than the horizontal, the vertical wave number, m, dominates the expression for the horizontal phase velocity, c_x, as given in Equation A2, and the determination of c_x is only slightly affected. The derived value of c_z, on the other hand, may be significantly lower than its true value.

Table 2 shows the results of analyzing all the periodic buoyancy waves seen on the SPO passes; Table 3 details the equivalent data for the isolated waves. The latter are particularly interesting as they may provide insight into the associated surface winds that are presumably exciting them [*Briggs and Leovy*, 1974].

Virtually no clouds observed during SPO were found below the Martian arctic circle at lat. ~65° N (Figure 1). Furthermore, only a dozen out of some 50,000 putative cloud echoes occurred with the sun more than about 5° above the horizon, suggesting that cloud particles seen by MOLA during this season were almost exclusively composed of CO_2 ice.

Appendix

(1) A general expression for the vertical pressure profile in a planetary atmosphere, assuming an ideal gas in hydrostatic equilibrium, may be derived as

$$P = P_0\left(1-\frac{z}{\alpha H_0}\right)^{\alpha},\ \alpha = \frac{T_0}{H_0 L} \qquad (1)$$

$L = -\partial T/\partial z$ is the lapse rate of the ambient temperature, z is the height, H is the vertical scale height and the subscript "o" refers to the corresponding values at $z = 0$. For a "wet" adiabat following the CO_2 vapor pressure curve, $L_w \approx 0.85$K km^{-1}; for a dry adiabat, $L_d = 4.3$K km^{-1}.

(2) Buoyancy waves [*Holton*, 1992] propagate with horizontal and vertical phase speeds relative to the mean wind, of c_x and c_z, respectively, where

Table 3: Characteristics of Isolated Clouds—some of which may correspond to buoyancy waves (possibly lee waves). "Height" is the maximum altitude above the surface of the echoes seen.

Orbit Number	Lat ° N	Lon ° E	Intrinsic Period sec	Height km
203	64	9	3492	3.9
203	63	8	N / A	4.3
214	53	290	N / A	2.4
215	85	251	N / A	5.6
215	85	165	N / A	8.6
219	74	168	N / A	7.8
219	66	163	N / A	1.6
220	81	10	3492	1.3
222	63	11	5907	2.0
225	77	230	3114	4.6
230	74	94	N / A	2.5
236	84	283	3915	3.5
236	85	193	4121	5.5
242	77	214	N / A	1.5
242	67	206	N / A	2.9
257	86	235	4146	5.2
257	82	190	5275	3.1
264	77	216	3425	7.0
264	85	180	2423	6.3
331	85	294	N / A	2.1
331	85	289	4121	1.7
331	82	191	N / A	4.2
333	71	194	N / A	7.7
335	79	4	N / A	6.8
335	83	237	N / A	9.4
340	77	88	N / A	4.1
349	79	359	N / A	8.7
353	81	46	3225	1.6
360	81	291	4937	6.2
369	85	221	N / A	3.5
371	86	313	N / A	5.4
371	85	246	5664	4.0
372	77	190	N / A	5.1
376	86	184	N / A	4.6
389	81	36	N / A	2.3
390	86	269	3672	3.8
390	85	249	5958	2.7
391	81	56	4073	2.9
392	85	351	N / A	1.2
396	79	62	N / A	5.2
396	81	58	N / A	5.2
396	82	288	4272	4.1
409	80	8	N / A	1.9
409	80	8	N / A	2.1
411	80	27	N / A	3.6
411	80	26	N / A	2.9
419	85	354	N / A	2.1
422	83	303	N / A	1.8
422	85	205	N / A	2.7
424	72	345	N / A	2.4
435	85	231	N / A	2.9
437	85	177	N / A	2.4
455	84	339	N / A	6.6

$$c_x = \frac{\hat{\nu}}{k},\ c_z = \frac{\hat{\nu}}{m},\ \hat{\nu} = \frac{Nk}{\sqrt{k^2 + m^2}} = N\cos A \quad . \quad (2)$$

$\hat{\nu}$ is the intrinsic frequency of oscillation, k and m are, respectively, the horizontal and vertical wave numbers, related to the observed horizontal and vertical wavelengths, λ_x and λ_z by $k = 2\pi/\lambda_x$ and $m = 2\pi/\lambda_z$, N is the buoyancy frequency (see Table 1), and A is the tilt angle of the wavefront slope as measured from the vertical.

Acknowledgments. We express appreciation for the dedicated assistance rendered by the MOLA engineering team and by Joan Quigley, in acquiring, processing and calibrating the MOLA data. The MOLA investigation is supported by NASA's Mars Surveyor Program.

References

Albee, A. A., F. D. Palluconi, and R. E. Arvidson, Mars Global Surveyor mission: overview and status, *Science, 279*, 1671-1672, 1998.

Briggs, G. A., and C. B. Leovy, Mariner 9 observations of the Mars north polar hood, *Bull. Amer. Meteorol. Soc., 55*, 278-296, 1974.

Hess, S. L., J. A. Ryan, J. E. Tillman, R. M. Henry and C. O. Leovy, The annual cycle of pressure on Mars measured by Viking Landers 1 and 2, *Geophys. Res. Lett., 7*, 197-200, 1980.

Holton, J. R., An introduction to dynamic meteorology, 3rd ed., p. 198, Acad. Press, San Diego, 1992.

Kahn, R., The spatial and seasonal distribution of Martian clouds, and some meteorological implications, *J. Geophys. Res., 89*, 6671-6688, 1984.

Mie, G., Beiträge zur Optik trüber Medien, speziell kolloida-ler Metallösungen, *Ann. der Physik, 25*, 377-446, 1908.

Murphy, J. R., O. B. Toon, R. M. Haberle, and J. B. Pollack, Numerical simulations of the decay of Martian global dust storms, *J. Geophys. Res., 95*, 14629-14648, 1990.

Smith, D. E., M. T. Zuber, *et al. (12 authors)*, Topography of the northern hemisphere of Mars from the Mars Orbiter Laser Altimeter, *Science, 279*, 1686-1692, 1998.

Zuber, M. T., D. E. Smith, S. C. Solomon, D. O. Muhleman, J. W. Head, J. B. Garvin, J. B. Abshire, and J. L. Bufton, The Mars Observer Laser Altimeter investigation, *J. Geophys. Res., 97*, 7781-7797, 1992.

Zuber, M. T., D. E. Smith, S. C. Solomon *et al. (21 authors)*, Observations of the north polar region of Mars from the Mars Orbiter Laser Altimeter, *Science, 282*, 2053-2060, 1998.

Zurek, R. W., J. R. Barnes, R. M. Haberle, J. B. Pollack, J. E. Tillman, and C. B. Leovy, Dynamics of the atmosphere of Mars, in *Mars*, edited by H. H. Kieffer, B. M. Jakosky, C. W. Snyder, and M. S. Matthews, pp. 835-933, Univ. of Ariz. Press, Tucson, 1992.

G. H. Pettengill and P. G. Ford, Center for Space Research, Massachusetts Institute of Technology, Cambridge, MA 02139 (e-mail: ghp@space.mit.edu, pgf@space.mit.edu).

(Received July 1, 1999; revised September 15, 1999; accepted October 22, 1999.)